ACS APPLIED MATERIALS & INTERFACES

Research Article

www.acsami.org

Effect of Water Sorption on the Electronic Conductivity of Porous Polymer Electrolyte Membrane Fuel Cell Catalyst Layers

David R. P. Morris, Selina P. Liu, David Villegas Gonzalez, and Jeff T. Gostick*

Department of Chemical Engineering, McGill University, H3A 2B2 Montreal, Québec, Canada

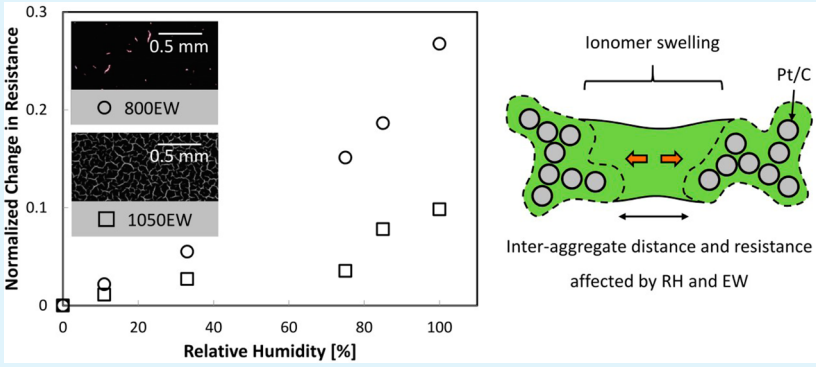

ABSTRACT: A method is described for measuring the effective electronic conductivity of porous fuel cell catalyst layers (CLs) as a function of relative humidity (RH). Four formulations of CLs with different carbon black (CB) contents and ionomer equivalent weights (EWs) were tested. The van der Pauw method was used to measure the sheet resistance (R_S), which increased with RH for all samples. The increase was attributed to ionomer swelling upon water uptake, which affects the connectivity of CB aggregates. Greater increases in R_S were observed for samples with lower EW, which uptake more water on a mass basis per mass ionomer. Transient R_S measurements were taken during absorption and desorption, and the resistance kinetics were fit using a double exponential decay model. No hysteresis was observed, and the absorption and desorption kinetics were virtually symmetric. Thickness measurements were attempted at different RHs, but no discernible changes were observed. This finding led to the conclusion that the conducting Pt/C volume fraction does not change with RH, which suggests that effective medium theory models that depend on volume fraction alone cannot explain the reduction in conductivity with RH. The merits of percolation-based models were discussed. Optical micrographs revealed an extensive network of "mud cracks" in some samples. The influence of water sorption on CL conductivity is primarily explained by ionomer swelling, and its effects on the quantity and quality of interaggregate contacts were discussed.

KEYWORDS: *composite, microstructure, percolation, ionomer, swelling, kinetics, aggregate, tunneling*

1. INTRODUCTION

The catalyst layers (CLs) typically used in polymer electrolyte membrane fuel cells (PEMFCs) are thin (≈1−20 μm), porous electrodes that consist of catalyst nanoparticles (typically platinum), supported on carbon black (CB) particles (≈20−50 nm), dispersed in an ionomer matrix. CB particles used in CLs tend to form branched agglomerates of ≈100−300 nm[1−3] that are surrounded by an ultrathin (≈1−25 nm) layer of ionomer[1,4−7] and form larger-scale porous aggregates of ≈1−3 μm (note fuel cell terminology is used here, which conflicts with the generally accepted conventions[2,8]). CLs are more structured than a typical CB−polymer composite since they are porous, which means that the agglomerates and aggregates are further segregated within the solid phase, as shown schematically in Figure 1.

The CLs play a central role in fuel cell operation as they catalyze the electrochemical reactions between protons, electrons, and gaseous reactants. The phases of the CL form percolating networks, each of which supports one or more

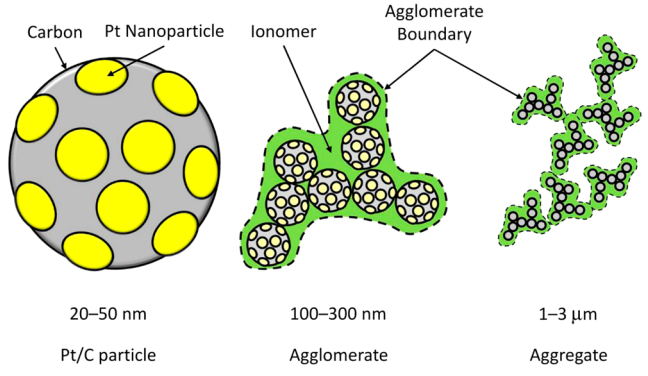

Figure 1. Schematic diagram of the CL composite microstructures.

Received: June 3, 2014
Accepted: October 2, 2014
Published: October 2, 2014

Table 1. Catalyst Layer Characteristics[a]

	$\rho_{A,Pt}$ [mg cm^{-2}]	w_{ion}	w_{ion}/w_C	$\phi_{Pt/C}$	t [μm]
800+C	0.241−0.273	0.402	1.05	0.142 ± 0.015	22.1 ± 1.8
850−C	0.242[b]	0.323	1.00	0.115 ± 0.005	11.8 ± 0.6
1050−C	0.260−0.320	0.365	1.20	0.125 ± 0.008	12.6 ± 0.6
1050+C	0.236[b]	0.400	1.00	0.108 ± 0.003	27.9 ± 0.6

[a]Uncertainty denotes standard deviation. [b]Representative value.

transport mechanisms: the network of Pt/C particles conducts electrons; the ionomeric binder conducts protons; and reactant oxygen and hydrogen gases and product water vapor and liquid travel through the void space. Experimental measurement of the transport properties in each of these phases is of great value for fuel cell manufacturers and researchers alike. It has been pointed out that since the electronic conductivity is at least an order of magnitude higher than the protonic conductivity of the ionomer phase it has little bearing on fuel cell operation,[9−11] but this view is too narrow for several reasons. A quick and reliable method for measuring conductivity provides a useful performance metric when designing CL structures as well as for quality control purposes. CL conductivity measurements are also valuable forensic tools for assessing things like carbon corrosion[12] and other structural degradation of the CL caused by operation. Moreover, CLs are prone to incur structural defects, such as cracks,[6,13,14] either through the manufacturing process or through operational wear, which lead to large differences between samples that can be characterized by electrical conductivity tests. Finally, modeling the complex, interacting phenomena in the CL requires accurate knowledge of all transport parameters including conductivity, especially for modeling at the pore scale where the distribution of phases greatly impacts overall behavior.

CLs are inherently difficult to study. They are very thin, making it difficult to apply controlled boundary conditions or to measure variables at specific locations; they are not self-supporting, meaning that sample mounting and sample holder design is a major challenge for any experimental technique; they are also quite fragile and can be damaged by contact (e.g., electrode leads or oxygen probes). Furthermore, although it is common to generalize CLs as a homogeneous media when applying transport laws on the scale of a fuel cell, CLs are highly heterogeneous on the microscopic level at which transport occurs. The transport properties of CLs are highly dependent on the structure of the percolating networks, but structural properties are a challenge to measure or even visualize due to the very small length scales (in the 10−100 nm range).[1,4] Finally, one of the most challenging aspects of studying CLs is the water-absorbing behavior of the ionomer material—usually a perfluorosulfonic acid (PFSA) polymer such as Nafion. In a working fuel cell, water is present in the CLs as a result of humidified reactants and generation via the oxygen reduction reaction in the cathode. Kusoglu et al.[15] recently presented ellipsometry data that confirm that ultrathin (<100 nm) ionomer films swell when exposed to water vapor. Ionomer swelling can result in alteration of the CL microstructure,[6,16] e.g., by invasion of the ionomer into the void space[17] and separation of CB particles from one another,[9,18,19] as well as delamination of layers in the fuel cell.[14] Consequently, it is necessary to include the effects of ionomer swelling when studying any transport process in the CL.

In this work, the van der Pauw (VDP) method[20] was used to measure the electronic conductivity of the Pt/C network in several different CLs. The VDP method has been applied to gas diffusion layer materials typically found in fuel cells,[21] and it generally excels at measuring in-plane conductivity of thin layers.[22] A simple adaptation of this technique in the present work was to enable measurements at variable levels of relative humidity (RH). The CL conductivity was found to vary substantially with RH, despite the obvious fact that the intrinsic electronic conductivity of Pt/C particles is not affected by the RH of the environment. The observed influence of RH on electrical conductivity is presumably a result of structural changes in the CL caused by ionomer swelling leading to rearrangement of the Pt/C particle network.[9,16,18,19,23] Indeed, this effect has been studied in the Nafion−carbon nanotube[24] and other polymer−CB composites for sensor applications.[19,23,25] Thus, the electrical conductivity method reported here is of direct interest not only for model validation and performance characterization purposes but also as a valuable source of information about CL structure, interfacial phenomena, and percolation properties.

2. EXPERIMENTAL SECTION

2.1. Sample Fabrication and Characterization. In general, CLs are made by applying a colloidal ink either onto the surface of an ionomer membrane or onto a polytetrafluoroethylene (PTFE) substrate and then transferred onto the membrane, known as the decal transfer method. The ink consists of CB-supported Pt nanoparticles and a dissolved ionomer in a solvent. At the outset of this experiment, attempts were made to measure the conductivity of CLs in their natural state as part of a membrane electrode assembly (MEA). When current was applied, however, the measured voltage drop across the sample tended to drift with time. It was hypothesized that the electric field present in the CL induced migration of protons in the ionomer, which in turn altered the electric field experienced by the electrons. To avoid this apparent capacitive charging effect, samples were tested in decal form, i.e., applied to a sheet of PTFE, which eliminated the transient behavior but led to highly inconsistent results owing to the fragile nature of the CL on a flexible decal backing. Applying the CLs to a rigid glass microscope slide remedied all such problems. Of course, the interaction between the ionomer and the substrate will affect the ionomer agglomeration[7] in the CL and therefore possibly the CL microstructure as well. Ionomer−substrate interaction can also affect the water sorption[26] and swelling properties[15] of the ionomer, such that the results presented here will likely differ from those obtained using a different substrate. The CL ink was applied to glass slides (3 in. × 1 in.) using a Mayer bar technique, also known as a drawdown bar technique, which consists of a stainless steel metering rod that is wound tightly with stainless steel wire of varying diameter. The catalyst ink is applied to the edge of the substrate, and the Mayer bar is rolled over the ink to distribute it across the length of the substrate by a motorized drawdown table.

In order to investigate the effects of ionomer type and carbon content on conductivity and swelling behavior, four different material recipes were used, and samples were fabricated in triplicate. There are high- and low-carbon loading formulations (denoted "+C" and "−C," respectively) and high- and low-ionomer equivalent weight (EW) (1050 and 800/850, respectively) formulations. The ionomers used in this study were either Nafion 850 EW or 1050 EW (Dupont) or 800

EW PFSA (3M). EW [g mol^{-1}] is the mass of ionomer per sulfonate group. The CL characteristics, namely, the Pt loading $\rho_{A,Pt}$ [mg cm^{-2}], ionomer weight fraction w_{ion}, ionomer-to-carbon ratio w_{ion}/w_C, estimated Pt/C volume fraction $\phi_{Pt/C}$, and thickness t [μm], are provided in Table 1. Commercial Pt/C particles were obtained from Tanaka Kikinzoku Kogyo K.K. (TKK, Tokyo, Japan). Since the same type of carbon was used in all samples, parameters such as the particle size, intrinsic particle conductivity, particle density, and surface chemistry should be constant between formulations. The BET surface area of the CB used was >700 m^2 g^{-1}.

2.1.1. Optical Micrographs. One of the key features of most of the formulations was the presence of a crack network as seen in the optical micrographs in Figure 2 obtained using a microscope camera

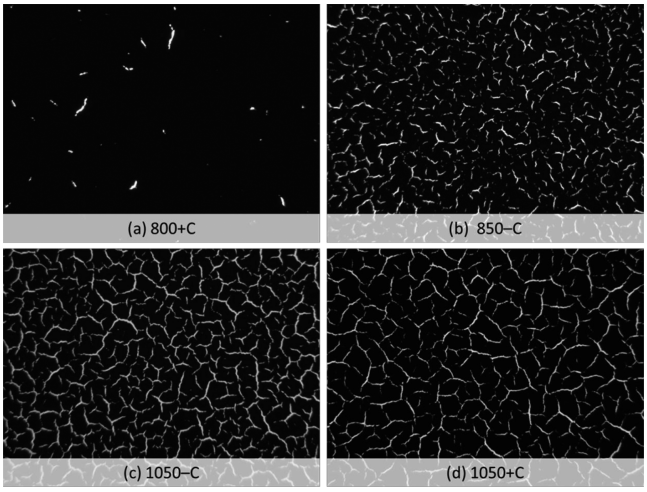

Figure 2. Optical micrographs of samples (a) 800+C, (b) 850−C, (c) 1050−C, and (d) 1050+C at 40× magnification. Each image represents a 1.66 × 1.24 mm^2 area.

(Infinity1, Lumenera) with a Diaplan optical microscope (Leitz). It is somewhat surprising that conductive paths exist across the entire samples given the extent of the cracks. Image analysis in ImageJ, however, shows that the Pt/C phase (black) actually consists of a single large connected cluster with only a few isolated islands near the edges. These islands would presumably be connected to the main cluster if the image were larger. The crack network, sometimes referred to as "mud cracks", has been described in the literature,[14] and the images are similar to those obtained by Suzuki et al.,[13] who coated CL ink onto sheets of PTFE and Kusoglu et al.[6] who applied CLs onto porous PTFE membranes. The differences in crack structure are presumably the result of CB−ionomer interaction.[7,27,28] The implication of these cracks is that the conductivity values reported for a given sample are valid only for samples with similar (i.e., statistically identical) crack structures. Unfortunately, this rules out the side-by-side comparison of samples here. Attempts were made to capture images of wet and dry images by placing a sample equilibrated at 100% RH under the microscope allowing it to equilibrate to room conditions (≈30−50% RH) for several hours. No changes in the crack network were observed, meaning that at least a given sample can be compared with itself at different RH values.

2.1.2. Profilometry. The sample thickness was measured using a stylus profilometer (Veeco Dektak 3 Profiler). Other methods of surface characterization are more accurate, but the instrument resolution (≈1 nm) was superfluous for measuring the thickness of CLs (i.e., 10−20 μm). An example of a typical thickness profile is shown in Figure 3. A small region of the CL was scraped off to expose the glass slide substrate, which provided the baseline for the thickness measurements. The thickness was fairly uniform away from the spike near the scraped edge, and an average over at least 2 mm was used to get the reported values. Attempts were made to perform profilometry measurements on samples after being held at different RH values for

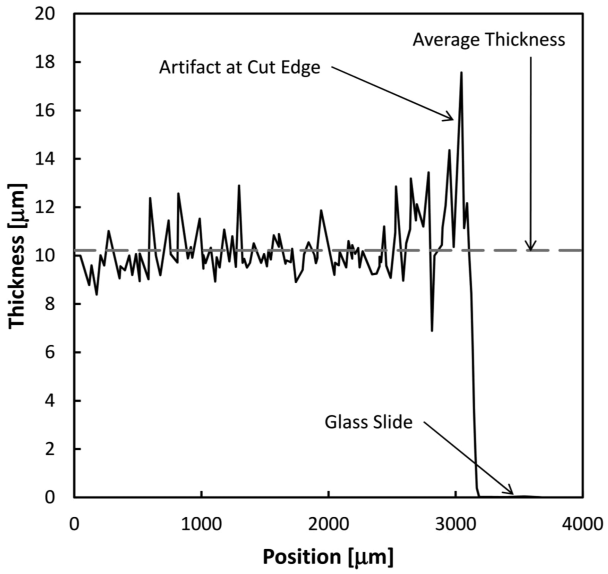

Figure 3. Thickness profile of CL applied to a glass slide, with a portion of the sample removed so the slide could provide a baseline for thickness measurements.

extended periods. The profilometer used did not have an environmental stage to maintain RH of the sample during testing. Measurements were taken quickly, and only 0% and 100% RH-equilibrated samples were tested to ensure maximal differences in thickness; however, no differences were observed. This key result is discussed in more detail later.

2.2. Experimental Setup. *2.2.1. van der Pauw Method.* For an isotropic material, electrical conductivity σ [S m^{-1}] is a scalar parameter that is related to the d.c. resistance R and the dimensions of a material by

$$\sigma = \frac{1}{R}\frac{L}{A} = \frac{1}{R}\frac{L}{Wt} \quad (1)$$

where A is the cross-sectional area of the sample; L is the length; W is the width; and t is the thickness. For thin, isotropic materials, such as CLs, it is convenient to use the sheet resistance R_S, which does not require a thickness measurement, which can be difficult to measure and is error-prone.[21] R_S is related to the average in-plane conductivity σ_{IP} of the sample by

$$R_S = \frac{1}{\sigma_{IP} t} \quad (2)$$

Because CLs are macroscopically isotropic, the in-plane and bulk conductivities are equivalent, i.e., $\sigma_{IP} = \sigma$.

R_S was determined in this work using the van der Pauw (VDP) method, which consists of a four-point probe setup arranged in a square array lying on the sample perimeter. The resistance of the sample was measured in two perpendicular directions, represented by x and y. The VDP equation relates the measured VDP resistances in the perpendicular x and y directions R_x and R_y with R_S, which is found by the iteration of[20]

$$\exp\left(-\frac{\pi R_x}{R_S}\right) + \exp\left(-\frac{\pi R_y}{R_S}\right) = 1 \quad (3)$$

To reduce experimental error, the resistance was measured along all four edges, rather than just two, and averages for R_x and R_y are used. The VDP method is advantageous for the study of CLs because it is noninvasive and the small probes are placed on the perimeter of the sample, so the likelihood of mechanical deformation of the CL by the probes is reduced. This is in contrast to the often used linear four-point probe (4PP) method,[29] which requires contact in the middle of the sample and over the entire sample width. Moreover, the distance

between the voltage probes must be accurately measured to calculate the conductivity using the 4PP method. The VDP method does not require any such dimensional measurement, and in fact, the VDP method is suitable for thin samples of any shape and size. The VDP method also probes the conductivity of the entire sample in all directions, unlike the 4PP, which is direction-dependent and only measures a region of a sample,[21] and it is thus subject to inhomogeneity and local defects.[22]

2.2.2. Sample Holder and Mounting. A custom sample holder for measuring the electrical conductivity of CLs as a function of RH was designed and built as shown in Figure 4. The three recesses above the

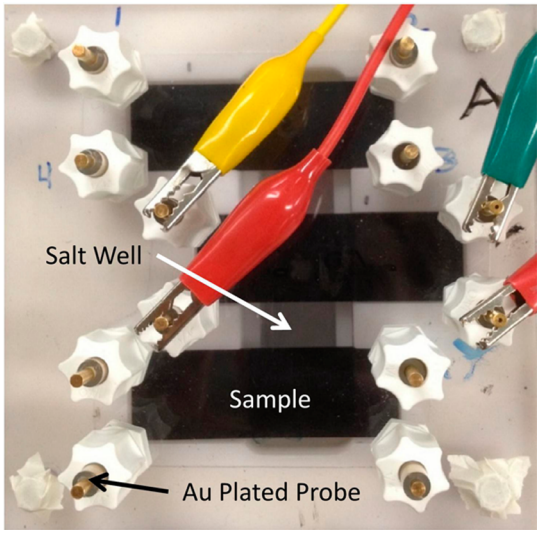

Figure 4. Schematic of the CL holder.

base held the CL-coated glass slides. The base plate below the samples contained a cavity for holding saturated salt solutions, which were used to control the RH in the chamber (LiCl = 11%, $MgCl_2$ = 33%, NaCl = 75%, KCl = 85%). A desiccant (Drierite) was used when a 0% RH environment was required, and reverse osmosis water was used for 100% RH tests. An RH probe (SHT75, Sensirion AG, ±1.8% RH accuracy) was fitted into one of the holders to confirm that the salt solutions did indeed provide the desired RH. Four 1/8-in. cylindrical gold-plated copper probes were used as leads on each corner of the sample. To maintain a constant RH inside the holder, probes were sheathed inside vinyl tubing and connected through polypropylene compression fittings. Each probe rested on the corner of the slides. To improve electrical contact between the CLs and the probes and to ensure that any damage to the CL caused by the probe contacts did not lead to discontinuity in the CL, the corners of the CL under probe tips were coated using a silver pen (MG Chemicals). Coating the CL directly with a conductive paste may also mitigate some errors induced by surface roughness.[25] The apparatus was sealed using silicone rubber gaskets. All tests were performed at ambient temperatures of approximately 22 °C.

2.2.3. Procedure. A power supply (Tektronix PWS4323) was used to provide a constant d.c. current to the CL samples. The applied current was confirmed using an independent reading of the voltage drop across a resistor using a data acquisition device (DAQ, Cole Parmer 18200−20) with 16-bit resolution (0.1% d.c. voltage accuracy (FS: 2 V)). The electrical potential drop across the other two electrodes was measured using a digital multimeter (Tektronix DMM 4020) with 0.01% d.c. voltage accuracy (FS: 200 mV). The current was varied between 0.1 and 10.0 mA, and the voltage was recorded for at least five different current levels per direction. Selection of the current and step size depended on the sample resistance. The results at each current gave the same resistance value within experimental accuracy of the equipment and were used only to provide an average value. Readings were taken within 5 s of current injection to mitigate ohmic heating effects. A representative transient voltage response to the current pulses is provided in Figure 5. The voltage data presented in Figure 5 were collected using the DAQ device rather than the DMM because the DAQ device has a much higher sampling rate.

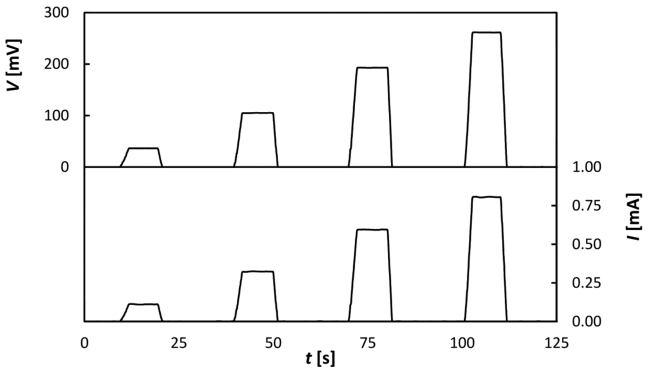

Figure 5. Transient voltage response to current pulses for a dry sample of 1050−C CL.

After collecting the data for one probe configuration, the electrode configuration was changed by switching two diagonally opposed electrodes using a relay array. The process was repeated to yield measurements in two orthogonal directions. The little anisotropy that was observed (<10%) can be attributed to minor defects in the CLs. Additional measurements from the other electrode pairs were taken to reduce experimental error, and the difference between the pairs of data from parallel directions was negligible.

2.2.4. Equilibration Time. All samples were allowed to equilibrate with the environment inside the holder for at least 24 h prior to performing experiments. It was confirmed that this duration was sufficient by measuring the sample R_S at periodic intervals for 24 h. The resistance kinetics of absorption and desorption are discussed later. Saab et al.[18] provided a much longer period (>5 days) for CLs to equilibrate and also showed an increase in resistance upon exposure to water using electrochemical impedance spectroscopy, but the resistance reached a maximum at 40 min of water exposure and actually decreased afterward. This effect was attributed to two parallel resistances (electronic and ionic) changing in opposite ways at different rates. The VDP method used in this study relies on d.c. measurements that measure the total conductivity of a sample. However, because the ionic conductivity of the CL is orders of magnitude lower than the electronic conductivity, the VDP method effectively measures only the electronic conductivity of the CL samples.[30] This is demonstrated in the voltage response to the current pulses in Figure 5, which clearly shows that there is virtually no capacitive effect.

3. RESULTS

3.1. Effective Conductivity. The effective transport properties in composite materials depend on: (1) the relative amount of each constituent component, usually expressed as volume fraction; (2) the pure component properties; and (3) the spatial distribution of the phase within the composite. In PEMFC CLs, for instance, effective electronic conductivity σ_{eff} occurs exclusively through the Pt/C phase, as neither the ionomer nor the void space conducts electrons.

The most common approximation of σ_{eff} of porous media is the Bruggeman approximation, which when applied to CLs is[5,11,29,31]

$$\sigma_{eff} = \sigma_{Pt/C}(\phi_{Pt/C})^{1.5} \quad (4)$$

where $\sigma_{Pt/C}$ is the conductivity through a single Pt/C particle, and $\phi_{Pt/C}$ is the volume fraction of the bulk carbon in the CL. The Bruggeman approximation is an example of an effective

medium approximation, where only the most basic structural information is considered.[32] Das et al.[11] proposed the use of another effective medium approximation, the Hashin−Shtrikman sphere approximation, to model transport properties of CLs

$$\sigma_{Pt/C} - \lambda_s \frac{3(1-\phi_{Pt/C})\sigma_{Pt/C}}{3-\phi_{Pt/C}} \geq \sigma_{eff} > 0 \quad (5)$$

where λ_s is the solid-phase geometry factor bounded by

$$\frac{3-\phi_{Pt/C}}{3(1-\phi_{Pt/C})} > \lambda_s \geq 1 \quad (6)$$

The Hashin−Shtrikman model assumes that the medium is a binary composite composed of coated polydisperse spheres, which is a fair approximation of CL structure. Although it is somewhat more physical than the Bruggeman model, the Hashin−Shtrikman model is ultimately an effective medium approximation, and it gives trends that are similar to the Bruggeman model.

More rigorous descriptions of effective transport properties in composites have been derived from percolation theory, which better includes the effects of structure and connectivity of the conducting components.[32] In random composite systems, a percolation threshold is reached when the volume fraction of the conducting phase reaches some critical value ϕ_c. At volume fractions below ϕ_c, the conducting particles are isolated from each other and surrounded by the insulating phase. In terms of CL design this situation would lead to a problematic underutilization of catalyst material since particles need electrical access to function. Applying the most basic form of percolation theory to the CL[1,23,27,32−35] results in

$$\sigma_{eff} \propto \sigma_{Pt/C}(\phi_{Pt/C} - \phi_{c,Pt/C})^{\tau}, \ \phi_{Pt/C} \geq \phi_{c,Pt/C}$$
$$\sigma_{eff} = 0, \ \phi_{Pt/C} < \phi_{c,Pt/C} \quad (7)$$

where $\phi_{c,Pt/C}$ is the critical volume fraction of Pt/C particles, and τ is the critical exponent. For special cases, such as a uniform distribution of spheres, these parameters have so-called "universal" values of 0.16 and 2, respectively,[1,27,32,34,36] although other values have been reported for the CL.[5] In order to apply the appropriate percolation model, knowledge of the transport property behavior and an idea of the critical parameters ϕ_c and τ are necessary; hence, the Bruggeman model is used much more often.[5,11,37]

3.1.1. Volume Fraction Determination. The mass fraction of each component is much easier to control during fabrication than the volume fraction, so CL samples are generally referred to by their composition in terms of weight fractions. To discuss the conduction of the CL samples in terms of structure, it is necessary to convert known mass fractions to volume fractions as outlined below. The weight fraction summation for a dry CL is $w_{Pt/C} + w_{ion} = 1$, where $w_{Pt/C}$ is the weight fraction of the CB-supported Pt nanoparticles and w_{ion} is the weight fraction of the ionomer. The volume fraction summation for a dry CL is $\phi_{Pt/C} + \phi_{ion} + \phi_v = 1$, where $\phi_{Pt/C}$, ϕ_{ion}, and ϕ_v denote the volume fraction of the Pt/C, ionomer, and void phases, respectively. The Pt/C volume fraction can be determined as a function of other measurable or known quantities using the following relation[31,36−38]

$$\phi_{Pt/C} = \left(\frac{1}{\rho_{Pt}} + \frac{w_C}{w_{Pt}\rho_{CB}}\right)\frac{\rho_{A,Pt}}{t(\phi_{RH})} \quad (8)$$

where $\rho_{A,Pt}$ is the average areal Pt loading [mg Pt cm^{-2}]; ρ_{Pt} and ρ_{CB} are the densities of Pt and CB, respectively; and $t(\phi_{RH})$ is the thickness of the sample, which may be a function of the local RH ϕ_{RH}. All of the parameters in eq 8 are known *a priori* except for the thickness, which can be controlled or determined *a posteriori*.[37]

It is important to note that the density of the CB particles ρ_{CB} is not necessarily equivalent to that of bulk carbon ρ_C. In fact, CB particles are often hollow, giving them better intrinsic or specific conductivity.[23,27,33,39] Using a simple volume summation for a single CB particle ($V_{CB} = V_C + V_v$) along with the fact that the mass of the CB particle is equal to the mass of the carbon in the particle ($m_{CB} = m_C$), then

$$\frac{m_{CB}}{\rho_{CB}} = \frac{m_{CB}}{\rho_C} + V_v \quad (9)$$

which, when divided by m_{CB} gives

$$\frac{1}{\rho_{CB}} = \frac{1}{\rho_C} + \frac{V_v}{m_{CB}} = \frac{1}{\rho_C} + v_v \quad (10)$$

where v_v is the specific void volume or specific total (closed and open) pore volume of the CB [cm^3 g^{-1}]. The relationship between CB porosity, $\phi_{v,CB}$, density, and specific void volume is then

$$\rho_{CB} = \frac{\rho_C}{1 + v_v\rho_C} = \rho_C(1 - \phi_{v,CB}) \quad (11)$$

Given that ρ_C is 2 g cm^{-3} and that the CB particle density ρ_{CB} is often reported as 1.8 g cm^{-3}, a nominal CB porosity $\phi_{v,CB}$ is then 0.1.[40] Similar values are obtained for Vulcan XC-72 ($\phi_{v,CB} = 0.11$, $\rho_{CB} = 1.79$ g cm^{-3}).[41] The apparent density or bulk density—the density of the powder that includes interparticle voids—is different from the CB particle density.[31] The value of ρ_{CB} affects the calculated value of $\phi_{Pt/C}$, and it should be selected carefully.

The ionomer volume fraction can be calculated by

$$\phi_{ion} = \frac{w_{ion}(\phi_{RH})}{w_{Pt}}\left(\frac{1}{\rho_{ion}(\phi_{RH})}\right)\frac{\rho_{A,Pt}}{t(\phi_{RH})} \quad (12)$$

where w_{ion} and ρ_{ion} both depend on the local RH because of water absorption in the ionomer.[26] Given $\phi_{Pt/C}$ and ϕ_{ion}, ϕ_v can be found using the volume fraction summation. ϕ_v represents an important portion of the total volume ($\phi_v \approx 0.3-0.6$)[1] but of course contributes nothing to the weight fraction summation. ϕ_v comprises the primary and secondary porosity of the CL, i.e., the inter- and intra-aggregate voids, respectively, but generally does not include the internal/closed porosity of the CB particles, if any. This is because the internal porosity of CB is considered part of $\phi_{Pt/C}$ rather than ϕ_v when ρ_{CB} is used instead of ρ_C; otherwise $\phi_{Pt/C}$ is underestimated. Furthermore, the CB internal porosity does not participate in gas transport or the electrochemical reactions and ionomer does not penetrate into it,[1,38] so it should not be included in ϕ_v.[37] Reported porosity values in some numerical studies are very low ($\phi_v \approx 0.1-0.2$).[36,42] Such low values might be necessary to explain mass-transfer limitations but are probably not realistic. The calculated porosities of the CLs used in this study are all relatively high, $\phi_v \approx 0.6-0.8$, but not unreasonably so,

considering that a minimum of $\phi_v \approx 0.3-0.6$ is required for gas diffusion.[1]

3.1.2. Conductivity as a Function of Pt/C Volume Fraction. The conductivity data for dry (RH = 0%) and humidified (RH = 100%) samples are presented as a function of $\phi_{Pt/C}$ in Figure 6. Differences between the two data sets are discussed in a later section. Samples with greater $\phi_{Pt/C}$ are clearly better conductors, but it is rather surprising that there is a difference of almost 2 orders of magnitude between the highest and lowest conductors especially given the narrow range of $\phi_{Pt/C}$ between these samples. Interestingly, the two lowest conductivity samples both contained the 1050 EW ionomer, while the other two samples contained 800 or 850 EW ionomer. Visual inspection of Figure 2 reveals that the 1050 EW samples seem to have a much more pronounced crack network, with cracks appearing wider, longer, and more interconnected. This assessment is purely qualitative, of course, but it is easy to accept that the different crack structures contributed to the observed differences in sample conductivities. However, this effect is ambiguous: for instance, the 1050+C sample (Figure 2(d)) possesses a higher C loading by weight (w_C) and a less extensive crack network than 1050−C (Figure 2(c)), but its $\phi_{Pt/C}$ and conductivity are both lower. In any event, one can safely assert that different ionomers lead to different mesostructures. This suggests that the particle agglomeration on the nanoscale might also have been affected, but it is not possible to discern the effects of nanoscale agglomeration on R_S without somehow accounting for the cracks. It is left as an exercise for future work to either study CLs with no cracks or find a way to normalize the measurements for differences in cracks.

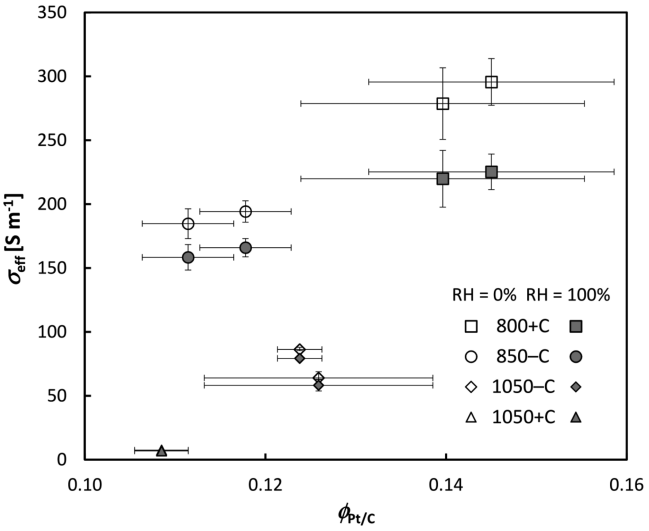

Figure 6. Conductivity of the four CL formulations under dry and humid conditions plotted versus conducting phase volume fraction. Error bars denote standard deviation.

Table 2 lists a selection of conductivity values reported in the literature. There is a large variation between these samples, but they all fall in the 1−400 S m^{-1} range, similar to the present work. Further comparisons between these values are not warranted considering the extensive mud cracks observed in the present samples, the possibility that cracks existed in the other studies, and the fact that different ionomers seem to have a large impact on the agglomeration behavior. Also shown in the bottom row of Table 2 is the conductivity of a common CB powder, Vulcan XC-72, which is almost a full order of magnitude higher than those of the CL materials, despite having a similar carbon volume fraction (reported as a packing fraction).[41] The addition of the electrically insulating ionomer, agglomeration and aggregation of the CB particles, and phase segregation resulting from the formation of pores all act to reduce the electronic conductivity of composites dramatically (by 2 orders of magnitude in some cases).

3.2. Sheet Resistance as a Function of Relative Humidity. The change in sheet resistance ($R_S - R_{S,0}$) normalized to the dry value ($R_{S,0}$) is presented as a function of RH for one of the replicate samples from each formulation in Figure 7. There is a moderate but distinct increase in R_S with RH for all samples, indicating that there is no transition from a conducting to an insulating composite, as has been observed for similar systems.[19,27,33,34] There is no doubt that the ionomer in the CL swells upon water sorption,[6] but it appears to have a modest impact on the structure of the conductive phase.

3.3. Resistance Kinetics. A representative R_S response during water absorption and desorption is presented for a sample of 1050−C in Figure 8. The data show that it takes >10 h to reach the equilibrium R_S value during absorption and desorption, $R_{S,\infty}$ (RH = 100%) and $R_{S,0}$ (RH = 0%), respectively. No hysteresis in R_S was observed between absorption and desorption experiments.

4. DISCUSSION

4.1. Conduction Mechanisms. In CB−polymer composites, electrons are forced to follow a limited number of paths between constricted interaggregate contacts, also known as the conductive backbone.[23] As discussed by Medalia,[33] Probst,[27]

Table 2. Experimental Data of the Electronic Conductivity of CLs and Vulcan XC-72 CB (Bottom Row)

reference	method	conditions	σ_{eff} [S m^{-1}]	$\phi_{Pt/C}$
this study	VDP	dry	7−300	0.105−0.15
Du et al.[42]	EIS	not provided	25−225	≈0.25−0.55
Gode et al.[9]	VDP	ambient	90−390	0.25−0.4
Saab et al.[18]	EIS	dry	≈130	≈0.3[a]
		40 min exposure	≈2.3	
		240 min exposure	≈2.9	
Siroma et al.[16]	Custom	25% RH	28	0.088
		80% RH	23	
Suzuki et al.[13]	4PP	not provided	10−100	≈0.25−0.4[a]
Pantea et al.[41] (Vulcan XC-72)	EIS	not provided	500−1000	0.3[b]

[a]Estimated. [b]CB packing fraction.

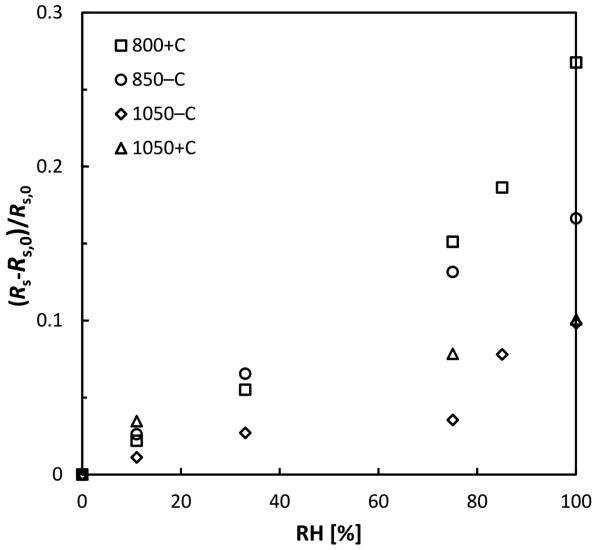

Figure 7. Normalized change in sheet resistance of the four CL formulations as a function of RH.

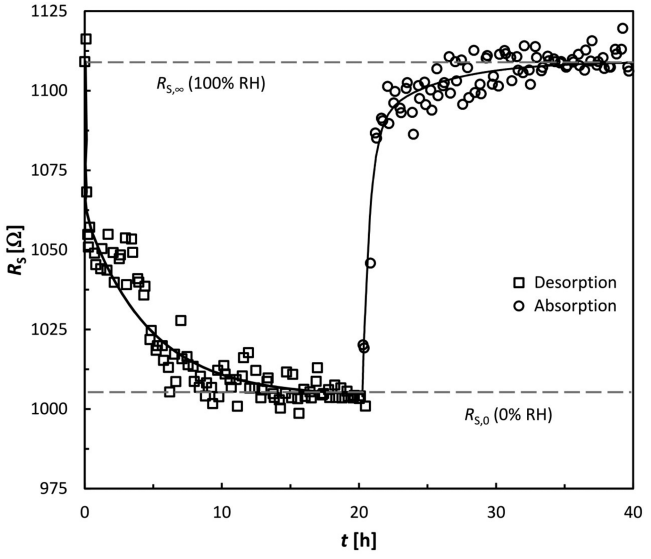

Figure 8. Transient sheet resistance response of a saturated sample of 1050–C CL that was dried (desorption) and then humidified (absorption).

and Zhang,[28] the resistance of CB–polymer composites depends on both the quantity and quality of contacts between aggregates. The effect of quantity of contacts is predicted by percolation theory: in general, a greater quantity of contacts fosters more conduction paths, which reduces the resistance of the composite. The quantity of contacts is also in part governed by the amount of conductive material in the composite ($\phi_{Pt/C}$), but the aggregate structure arguably has a greater effect.[27] The quality of contacts is essentially determined by the interparticle contact resistance, which is affected by the contact area, interparticle distance, and other surface properties.[23] The relative importance of quantity and quality of contacts is debated, and many models have been proposed to account for these parameters. A comprehensive review was conducted by Lux.[43] The effect of water absorption on the quantity and quality of contacts is discussed below.

4.2. Effect of Water Sorption on CL Conductivity. Water sorption clearly affects the conductivity of the CL. Soboleva et al.[44] used vapor sorption experiments to show that virtually all of the water absorbed by the CL is absorbed by the ionomer and not the CB particles. Therefore, even though electrons can be captured by water molecules on the CB surface,[28] the effect of surface hydration of CB particles on CL conductivity is likely minimal.

Water absorption by the ultrathin ionomer phase can induce several changes[45] that may affect conduction in the CL. The most obvious effect is ionomer swelling,[15] which can cause CB particle reorientation or migration, thereby disrupting the conductive backbone. Other effects, such as changes to crystallinity[15] or dissolution,[45] are not well understood, especially for Nafion in ultrathin morphologies.[15] Indeed, even the relationships among basic properties such as particle conductivity, swelling, and (water) vapor concentration are also not well understood and are being explored, especially in CB/polymer sensor applications. The effect of ionomer swelling on conductivity is the most straightforward explanation, but other potential effects of water absorption mentioned above cannot be ruled out.

4.3. Dimensional Changes. Some have suggested that swelling of the ionomer phase leads to an increase in the overall CL thickness,[18] like in other CB–polymer composites[19] and porous electrodes.[46] An overall thickness change, or plane strain, translates directly into a decrease in $\phi_{Pt/C}$ by eq 8. The change in measured resistance of CLs caused by dimensional changes, based on the basic resistance equation (eq 1), is simply

$$\frac{R}{R_0} = \frac{(L/L_0)}{(W/W_0)(t/t_0)(\sigma_{eff}/\sigma_{eff,0})} \tag{13}$$

where the subscript 0 denotes the parameter in a dry state. Gomadam and Weidner[46] substituted σ_{eff} with the Bruggeman approximation (eq 4) for another class of porous electrodes. If the Bruggeman approximation is applied here and $\phi_{Pt/C}$ is substituted with its mass fraction relationship (eq 8) along with the assumption that the area ($L \times W$) remains constant, which is reasonable since the CL is physically adhered to the substrate, eq 13 simplifies to the following

$$\frac{R}{R_0} = \left(\frac{t}{t_0}\right)^{0.5} = \frac{R_S}{R_{S,0}} \tag{14}$$

According to this relationship, the observed increase in R_S of 25% would have required a thickness change of about 56%. For comparison, one of the few studies that directly measured swelling strain of bulk Nafion ionomer film found 10–20% change in thickness for ultrathin (4–120 nm) films adhered to carbon at room temperature.[15] The Bruggeman approximation is therefore inapplicable to the data. Moreover, profilometry measurements conducted in the present study revealed no discernible thickness change between 0 and 100% RH-equilibrated samples, albeit without an environmental chamber. This finding implies that $\phi_{Pt/C}$ is independent of RH since the bulk volume of the CL did not change appreciably. If $\phi_{Pt/C}$ does not change, then percolation theory requires that the structure of the Pt/C network is changing as the ionomer swells to account for the change in σ_{eff}. Furthermore, ionomer swelling must have resulted in encroachment onto the void space, so the

increase in ϕ_{ion} comes at the expense of the ϕ_v, which may affect other transport properties as well.

4.2.2. Ionomer Swelling. The effect of polymer swelling on conduction is well-established and has been explored for sensor applications of polymer−CB composites.[19,23,25] The effect is known as the positive vapor coefficient (PVC) effect, and it is not unlike the positive temperature coefficient (PTC) effect observed in polymer−CB systems, where the conductivity of the composite drops rapidly with temperature.[28,47] Some attribute the reduction in conductivity for both effects to a decrease in CB volume fraction, but, like the present case, a change in volume fraction cannot explain the drop in conductivity.[23,35,47]

Ionomer swelling can affect the contact resistance in a number of ways. The most obvious is a reduction of interparticle contact area, e.g., by encroachment on the interstitial space. Ionomer swelling can also cause particle migration, which increases the interparticle distance and affects conductivity. In fact, electrons can jump between particles that are not in direct contact through a mechanism known as electron tunneling.[27,28,33,34,39,48,49] According to this theory, conduction can occur between neighboring particles even if they are separated by an insulating film, provided it is sufficiently thin (on the order of nanometers). The tunneling conductivity σ_{tun} [S m^{-1}] is related to the average interparticle distance d by an exponential relationship[48,49]

$$\sigma_{tun} \propto \exp(-d) \tag{15}$$

The length scale of ionomer swelling in the CL is likely similar to that of tunneling conduction, i.e., on the order of nanometers,[49] considering that the CL film is about 1−25 nm thick[1,4−7] and swelling strain is on the order of 10−20%.[15] Tunneling is a well-established phenomenon,[27,28,34,39,48,49] and it seems to provide much needed insight into the mechanism of conduction of ionomer-coated CB particles.

4.2.3. Effect of Ionomer EW. More water is required to reach equilibrium for a CL with a lower EW ionomer,[6,26,50] as it corresponds to a higher sulfonate group density. Hence, CLs with lower EW ionomer can uptake more water and thus undergo more swelling to reach equilibrium, which in turn seemingly causes the R_S to increase to a greater extent. Indeed, R_S increases more for samples with lower ionomer EW as shown in Figure 7. For instance, 800/850 EW CLs exhibited an increase between 15 and 25% in R_S when exposed to water vapor, whereas the R_S of 1050 EW CLs increased by only 10%. Furthermore, the 800+C samples possessed a higher ionomer volume fraction (ϕ_{ion} = 0.16−0.17) than the 850−C samples (0.10) and exhibited a greater increase in R_S as well. The 1050 EW CLs possessed similar ϕ_{ion} (0.10 for 1050+C and 0.11−0.12 for 1050−C) and also exhibited similar increases in R_S. Therefore, both ϕ_{ion} and EW seem to have an effect on swelling and the resistance of the CL.

As illustrated in Figure 2, the 1050 EW samples possess much more extensive crack networks than that of the 800 EW sample, which does not seem to have a crack network so much as scratches from handling. The 1050 EW samples also possess a lower $\phi_{Pt/C,}$ so there are likely fewer interparticle contacts in the 1050 EW samples compared to the 800 EW samples. Furthermore, Kusoglu et al.[6] found that CL samples with cracks were more hydrophilic. A greater reduction in conductivity upon swelling would therefore be expected in the 1050 EW samples based on a reduction in the quantity of contacts alone. However, the opposite occurs: a greater reduction in conductivity is observed in the 800 EW samples. This finding suggests that the structural changes induced by ionomer swelling cause a drop in both the quality and quantity of contacts.[23] In addition, the present samples did not undergo a pronounced change in conductivity, such as a conductor−insulator transition, so the conductive backbones were not strongly affected by ionomer swelling.

4.3. Resistance Kinetics. The R_S kinetics are characterized by an initial rapid change, where 50% of the change in R_S is achieved in the first hour, followed by a slow evolution to the final value. Because of the two regions, a classic one-term exponential decay model provides a poor fit to the data. A double exponential decay model has been used to fit the swelling[15] and water absorption[51,52] (although not desorption) kinetics of bulk Nafion films. This expression also fits the present R_S kinetics remarkably well, as shown in Figure 8

$$\frac{R_S(t) - R_{S,0}}{R_{S,\infty} - R_{S,0}} = 1 - \varphi \exp\left(-\frac{t}{\tau_1}\right) - (1 - \varphi)\exp\left(-\frac{t}{\tau_2}\right) \tag{16}$$

where φ is the quasi-equilibrium point of two-stage kinetic models, and τ_1 and τ_2 are time constants. The R_S kinetics during desorption are modeled by switching the initial and final R_S values ($R_{S,\infty}$ and $R_{S,0}$).

The first region of the R_S response corresponds to rapid water uptake, whereas the second region is attributed to structural changes in the ionomer, particularly polymer relaxation. Interestingly, both the absorption and desorption R_S kinetics are well fit by the model because R_S depends on the CL microstructure, which is affected by both ionomer swelling and contraction. This finding is in contrast to water sorption kinetics studies[51,52] where only absorption is well modeled by eq 16 because the ionomer must swell to accommodate water, whereas desorption is not hindered by ionomer swelling/contraction and a single exponential decay is appropriate.

Values of φ were in the range of 0.4−0.8, although these values are approximate, given the limited data obtained in the first region. Satterfield and Benziger[51] obtained a value of 0.35 for φ for thicker (>50 μm) bulk Nafion membranes, whereas Kongkanand[52] found values in the range 0.4−0.6 for large RH steps for thinner (1−3 μm) Nafion membranes applied to gold. Higher φ values indicate that bulk swelling, rather than polymer relaxation, dominates the transient R_S response.[52] The time constants in the first and second regions were between 10^2 and 10^3 s and on the order of 10^4 s, respectively. The first time constants seem to match the values obtained by Kusoglu et al.[6] (20−1000 s), who applied a single exponential model to water absorption kinetics of CLs, which likely corresponded to the first region only. These time constants are much greater than those obtained by Satterfield and Benziger[51] or Kongkanand,[52] which was explained by the strong interfacial resistance in ultrathin films to water transport.[6]

4.4. Comparison of Conductivity Models. It is worthwhile to compare the models commonly used to describe conductivity in composites. This analysis is purely qualitative given the small number of data points available and the apparent importance of the crack pattern, but it does demonstrate something of interest. Conduction in polymer−CB composites depends on the amount and structure of the CB particles. As discussed above, $\phi_{Pt/C}$ is a decent general indicator of conductivity, but it does not provide any additional structural information. For instance, $\phi_{Pt/C}$ remains constant throughout

water absorption, but the conductivity decreases because the quality and quantity of interparticle contacts is disturbed. The Bruggeman approximation model (eq 4) cannot explain this RH-dependent conductivity because $\phi_{Pt/C}$ remains constant. Similarly, the structural parameter of the Hashin−Shtrikman model (eqs 5 and 6) is usually kept constant ($\lambda_s = 1$),[11] so it too cannot account for the drop in conductivity without a change in $\phi_{Pt/C}$. (If λ_s is optimized for every data point (see eq 6) it fits the data perfectly, but that is not particularly useful in this case.) Therefore, the only practically applicable model to this data is the percolation theory model.

As mentioned earlier, there are many "universal" values of τ and $\phi_{Pt/C,c}$ and they are system-dependent. For a random, 3-dimensional distribution of spheres these correspond to $\tau = 2$ and $\phi_{Pt/C,c} = 0.16$. No samples possessed $\phi_{Pt/C,c} > 0.16$. Classic percolation theory suggests that none of the samples should conduct as they do not form a contiguous conducting matrix. Because they do indeed conduct, it can be safely asserted that the samples do not possess a structure that is similar to a random distribution of spheres. Indeed, the samples are clearly phase-segregated on the mesoscale, as depicted in the optical micrographs of most samples (Figure 2). Phase segregation is also characteristic of so-called high-structure CB, which tends to be highly branched and where $\phi_{Pt/C,c} < 0.16$ is not uncommon.[34,35,39] High-structure CBs result in higher conductivity than low-structure CBs, even at the same loading in the composite,[39] which is another example of why the volume fraction alone is inadequate to describe the structure of composites. Application of percolation theory models to estimate CL transport properties is therefore encouraged, but more experimental data are required to determine the critical parameters. Furthermore, improvements to percolation theory are necessary to account for the effects of phase segregation, as well as swelling and related phenomena, on conductivity.

5. CONCLUSIONS

The relationship between electronic conductivity and water absorption was explored for porous PEMFC CLs. The R_S of all samples increased when exposed to water vapor. The ionomer EW had an effect on the magnitude of the R_S change during water absorption, which suggests that the differences in ionomer swelling strain caused the different R_S responses. The CLs also exhibited different mesoscale crack structures due to ionomer−CB interaction, despite possessing the same type of CB. The reversible increase in R_S is attributed to moderate structural changes in the conducting CB backbone induced by ionomer swelling. Both the quantity and quality of interaggregate contacts affect the CL conductivity. The findings have implications for CL design, as disconnection in the conducting network may leave isolated islands of aggregates that no longer conduct, leading to particles that are no longer electrocatalytically active and decreased catalyst effectiveness. Exposure to liquid water may have a stronger effect on CL conductivity. Conductivity measurements may also be very useful in probing the structure and interfacial phenomena of CLs, as it is extremely difficult to do so quantitatively.[3] Indeed, the R_S kinetics provided valuable insight into the swelling characteristics of the ionomer film and aggregate interaction in CLs. The R_S kinetics were well-modeled by a double exponential decay, similar to previous studies that investigated water absorption[51,52] and swelling[15] of Nafion films.

The conductivity results that were obtained are only applicable to a given sample, which underscores the utility of the proposed quick and accurate conductivity method for obtaining data on individual samples. The conductivity data fell under the same range as literature values (7−300 S m^{-1}, cf. 10−400 S m^{-1}), despite the relatively low $\phi_{Pt/C}$ and varied crack structure that the present samples possessed. $\phi_{Pt/C}$ is a decent general indicator of conductivity, but the use of effective transport property models that incorporate other structural parameters, such as percolation theory, is encouraged, especially considering the phase-segregated structure of CLs. Dimensional change in the thickness (plane strain) of the CL due to ionomer swelling was not detected, implying that the ionomer must swell into the pore space, which may affect other transport parameters.

AUTHOR INFORMATION

Corresponding Author

*E-mail: jeff.gostick@mcgill.ca.

Notes

The authors declare no competing financial interest.

ACKNOWLEDGMENTS

The authors gratefully acknowledge the financial support of the Automotive Fuel Cell Cooperation (AFCC) Corporation and the Eugenie Ulmer Lamothe (EUL) Fund of the Department of Chemical Engineering of McGill University. The authors would also like to thank Mr. Mickey Tam at AFCC for preparing the CL samples, Dr. Richard Leask for the use of the optical microscope, and Dr. Adamo Petosa for the use of calibration slides.

REFERENCES

(1) Eikerling, M. H.; Malek, K.; Wang, Q. Catalyst Layer Modeling: Structure, Properties and Performance. In *PEM Fuel Cell Electrocatalysts and Catalyst Layers*; Zhang, J., Ed.; Springer: New York, 2008; pp 381−446.

(2) Hess, W. M.; Herd, C. R., Microstructure, Morphology and General Physical Properties. In *Carbon Black: Science and Technology*, Second ed.; Donnet, J.-B.; Bansal, R. C.; Wang, M.-J., Eds.; Marcel-Dekker: New York, NY, 1993; Chapter 3, pp 89−174.

(3) Soboleva, T.; Zhao, X.; Malek, K.; Xie, Z.; Navessin, T.; Holdcroft, S. On the Micro-, Meso-, and Macroporous Structures of Polymer Electrolyte Membrane Fuel Cell Catalyst Layers. *ACS Appl. Mater. Interfaces* **2010**, *2*, 375−384.

(4) Sadeghi, E.; Putz, A.; Eikerling, M. Effects of Ionomer Coverage on Agglomerate Effectiveness in Catalyst Layers of Polymer Electrolyte Fuel Cells. *J. Solid State Electrochem.* **2014**, *18*, 1271−1279.

(5) Dobson, P.; Lei, C.; Navessin, T.; Secanell, M. Characterization of the PEM Fuel Cell Catalyst Layer Microstructure by Nonlinear Least-Squares Parameter Estimation. *J. Electrochem. Soc.* **2012**, *159*, B514−B523.

(6) Kusoglu, A.; Kwong, A.; Clark, K. T.; Gunterman, H. P.; Weber, A. Z. Water Uptake of Fuel-Cell Catalyst Layers. *J. Electrochem. Soc.* **2012**, *159*, F530−F535.

(7) Holdcroft, S. Fuel Cell Catalyst Layers: A Polymer Science Perspective. *Chem. Mater.* **2013**, *26*, 381−393.

(8) Nichols, G.; Byard, S.; Bloxham, M. J.; Botterill, J.; Dawson, N. J.; Dennis, A.; Diart, V.; North, N. C.; Sherwood, J. D. A Review of the Terms Agglomerate and Aggregate with a Recommendation for Nomenclature Used in Powder and Particle Characterization. *J. Pharm. Sci.* **2002**, *91*, 2103−2109.

(9) Gode, P.; Jaouen, F.; Lindbergh, G.; Lundblad, A.; Sundholm, G. Influence of the Composition on the Structure and Electrochemical Characteristics of the PEFC Cathode. *Electrochim. Acta* **2003**, *48*, 4175−4187.

(10) Wagner, F. T.; Yan, S. G.; Yu, P. T., Catalyst and Catalyst-Support Durability. In *Handbook of Fuel Cells: Advances in Electrocatalysis, Materials, Diagnostics and Durability*; Vielstich, W., Gasteiger, H. A., Yokokawa, H., Eds.; Wiley: West Sussex, UK, 2009; Vol. *5*.
(11) Das, P. K.; Li, X.; Liu, Z.-S. Effective Transport Coefficients in PEM Fuel Cell Catalyst and Gas Diffusion Layers: Beyond Bruggeman Approximation. *Appl. Energy* **2010**, *87*, 2785−2796.
(12) Baghalha, M.; Stumper, J.; Harvey, D.; Eikerling, M. Modeling the Effect of Low Carbon Conductivity of the Cathode Catalyst Layer on PEM Fuel Cell Performance. *ECS Trans.* **2010**, *28*, 113−123.
(13) Suzuki, T.; Murata, H.; Hatanaka, T.; Morimoto, Y. Analysis of the Catalyst Layer of Polymer Electrolyte Fuel Cells. *R&D Rev. Toyota CRDL* **2004**, *39*, 33−38.
(14) Kundu, S.; Fowler, M. W.; Simon, L. C.; Grot, S. Morphological Features (Defects) in Fuel Cell Membrane Electrode Assemblies. *J. Power Sources* **2006**, *157*, 650−656.
(15) Kusoglu, A.; Kushner, D.; Paul, D. K.; Karan, K.; Hickner, M. A.; Weber, A. Z. Impact of Substrate and Processing on Confinement of Nafion Thin Films. *Adv. Funct. Mater.* **2014**, *24*, 4763−4774.
(16) Siroma, Z.; Hagiwara, J.; Yasuda, K.; Inaba, M.; Tasaka, A. Simultaneous Measurement of the Effective Ionic Conductivity and Effective Electronic Conductivity in a Porous Electrode Film Impregnated with Electrolyte. *J. Electroanal. Chem.* **2010**, *648*, 92−97.
(17) Rong, F.; Huang, C.; Liu, Z.-S.; Song, D.; Wang, Q. Microstructure Changes in the Catalyst Layers of PEM Fuel Cells Induced by Load Cycling: Part I. Mechanical Model. *J. Power Sources* **2008**, *175*, 699−711.
(18) Saab, A. P.; Garzon, F. H.; Zawodzinski, T. A. Determination of Ionic and Electronic Resistivities in Carbon/Polyelectrolyte Fuel-Cell Composite Electrodes. *J. Electrochem. Soc.* **2002**, *149*, A1541−A1546.
(19) Lonergan, M. C.; Severin, E. J.; Doleman, B. J.; Beaber, S. A.; Grubbs, R. H.; Lewis, N. S. Array-Based Vapor Sensing Using Chemically Sensitive, Carbon Black-Polymer Resistors. *Chem. Mater.* **1996**, *8*, 2298−2312.
(20) Van Der Pauw, L. J. A Method of Measuring Specific Resistivity and Hall Effect of Discs of Arbitrary Shape. *Philips Res. Rep.* **1958**, *13*, 1−9.
(21) Morris, D. R. P.; Gostick, J. T. Determination of the In-Plane Components of the Electrical Conductivity Tensor in PEM Fuel Cell Gas Diffusion Layers. *Electrochim. Acta* **2012**, *85*, 665−673.
(22) Koon, D. W.; Knickerbocker, C. J. What Do You Measure When You Measure Resistivity? *Rev. Sci. Instrum.* **1992**, *63*, 207−210.
(23) Blythe, A. R.; Bloor, D. *Electrical Properties of Polymers*, 2nd ed.; Cambridge University Press: New York, 2005.
(24) Lee, K.; Lee, J.-W.; Kim, S.-I.; Ju, B.-k. Single-Walled Carbon Nanotube/Nafion Composites as Methanol Sensors. *Carbon* **2011**, *49*, 787−792.
(25) Lei, H.; Pitt, W. G.; McGrath, L. K.; Ho, C. K. Modeling Carbon Black/Polymer Composite Sensors. *Sens. Actuators, B* **2007**, *125*, 396−407.
(26) Morris, D. R.; Sun, X. Water-Sorption and Transport Properties of Nafion 117 H. *J. Appl. Polym. Sci.* **1993**, *50*, 1445−1452.
(27) Probst, N., Conducting Carbon Black. In *Carbon Black: Science and Technology*, 2nd ed.; Donnet, J.-B., Bansal, R. C., Wang, M.-J., Eds.; Marcel-Dekker: New York, NY, 1993; Chapter 8, pp 271−288.
(28) Zhang, W.; Dehghani-Sanij, A. A.; Blackburn, R. S. Carbon Based Conductive Polymer Composites. *J. Mater. Sci.* **2007**, *42*, 3408−3418.
(29) Zamel, N.; Li, X. Effective Transport Properties for Polymer Electrolyte Membrane Fuel Cells − With a Focus on the Gas Diffusion Layer. *Prog. Energy Combust. Sci.* **2013**, *39*, 111−146.
(30) Gomadam, P. M.; Weidner, J. W.; Zawodzinski, T. A.; Saab, A. P. Theoretical Analysis for Obtaining Physical Properties of Composite Electrodes. *J. Electrochem. Soc.* **2003**, *150*, E371−E376.
(31) Marr, C.; Li, X. Composition and Performance Modelling of Catalyst Layer in a Proton Exchange Membrane Fuel Cell. *J. Power Sources* **1999**, *77*, 17−27.
(32) Torquato, S. *Random Heterogeneous Materials: Microstructure and Macroscopic Properties*; Springer: New York, NY, 2002; Vol. *16*.
(33) Medalia, A. I. Electrical Conduction in Carbon Black Composites. *Rubber Chem. Technol.* **1986**, *59*, 432−454.
(34) Balberg, I. A Comprehensive Picture of the Electrical Phenomena in Carbon Black− Polymer Composites. *Carbon* **2002**, *40*, 139−143.
(35) Carmona, F.; Ravier, J. Electrical Properties and Mesostructure of Carbon Black-Filled Polymers. *Carbon* **2002**, *40*, 151−156.
(36) Wang, Q.; Eikerling, M.; Song, D.; Liu, Z.; Navessin, T.; Xie, Z.; Holdcroft, S. Functionally Graded Cathode Catalyst Layers for Polymer Electrolyte Fuel Cells: I. Theoretical Modeling. *J. Electrochem. Soc.* **2004**, *151*, A950−A957.
(37) Secanell, M.; Karan, K.; Suleman, A.; Djilali, N. Multi-Variable Optimization of PEMFC Cathodes Using an Agglomerate Model. *Electrochim. Acta* **2007**, *52*, 6318−6337.
(38) Siegel, N. P.; Ellis, M. W.; Nelson, D. J.; von Spakovsky, M. R. A Two-Dimensional Computational Model of a PEMFC with Liquid Water Transport. *J. Power Sources* **2004**, *128*, 173−184.
(39) Huang, J. C. Carbon Black Filled Conducting Polymers and Polymer Blends. *Adv. Polym. Technol.* **2002**, *21*, 299−313.
(40) Kühner, G.; Voll, M., Manufacture of Carbon Black. In *Carbon Black: Science and Technology*, 2nd ed.; Donnet, J.-B., Bansal, R. C., Wang, M.-J., Eds.; Marcel-Dekker: New York, NY, 1993; Chapter 1, pp 1−66.
(41) Pantea, D.; Darmstadt, H.; Kaliaguine, S.; Roy, C. Electrical Conductivity of Conductive Carbon Blacks: Influence of Surface Chemistry and Topology. *Appl. Surf. Sci.* **2003**, *217*, 181−193.
(42) Du, C. Y.; Shi, P. F.; Cheng, X. Q.; Yin, G. P. Effective Protonic and Electronic Conductivity of the Catalyst Layers in Proton Exchange Membrane Fuel Cells. *Electrochem. Commun.* **2004**, *6*, 435−440.
(43) Lux, F. Models Proposed to Explain the Electrical Conductivity of Mixtures Made of Conductive and Insulating Materials. *J. Mater. Sci.* **1993**, *28*, 285−301.
(44) Soboleva, T.; Malek, K.; Xie, Z.; Navessin, T.; Holdcroft, S. PEMFC Catalyst Layers: The Role of Micropores and Mesopores on Water Sorption and Fuel Cell Activity. *ACS Appl. Mater. Interfaces* **2011**, *3*, 1827−1837.
(45) Mauritz, K. A.; Moore, R. B. State of Understanding of Nafion. *Chem. Rev.* **2004**, *104*, 4535−4586.
(46) Gomadam, P. M.; Weidner, J. W. Modeling Volume Changes in Porous Electrodes. *J. Electrochem. Soc.* **2006**, *153*, A179−A186.
(47) Hindermann-Bischoff, M.; Ehrburger-Dolle, F. Electrical Conductivity of Carbon Black− Polyethylene Composites: Experimental Evidence of the Change of Cluster Connectivity in the PTC Effect. *Carbon* **2001**, *39*, 375−382.
(48) Balberg, I. Tunneling and Nonuniversal Conductivity in Composite Materials. *Phys. Rev. Lett.* **1987**, *59*, 1305.
(49) Balberg, I.; Azulay, D.; Toker, D.; Millo, O. Percolation and Tunneling in Composite Materials. *Int. J. Mod. Phys. B* **2004**, *18*, 2091−2121.
(50) Jalani, N. H.; Datta, R. The Effect of Equivalent Weight, Temperature, Cationic Forms, Sorbates, and Nanoinorganic Additives on the Sorption Behavior of Nafion®. *J. Membr. Sci.* **2005**, *264*, 167−175.
(51) Satterfield, M. B.; Benziger, J. B. Non-Fickian Water Vapor Sorption Dynamics by Nafion Membranes. *J. Phys. Chem. B* **2008**, *112*, 3693−3704.
(52) Kongkanand, A. Interfacial Water Transport Measurements in Nafion Thin Films Using a Quartz-Crystal Microbalance. *J. Phys. Chem. C* **2011**, *115*, 11318−11325.